SSM-based electrophysiology, a label-free real-time method reveals sugar binding & transport events in SGLT1

Andre Bazzone [a],[*],[1], Alexander Körner [b],[c],[1], Melanie Meincke [a], Manan Bhatt [a], Srujan Dondapati [b], Maria Barthmes [a], Stefan Kubick [b],[d],[e], Niels Fertig [a]

[a] *Nanion Technologies GmbH, Ganghoferstr. 70a, 80339, Munich, Germany*
[b] *Fraunhofer Institute for Cell Therapy and Immunology (IZI), Branch Bioanalytics and Bioprocesses (IZI-BB), Am Mühlenberg 13, 14476, Potsdam, Germany*
[c] *Institute of Biotechnology, Technische Universität Berlin, Gustav-Meyer-Allee 25, 13355, Berlin, Germany*
[d] *Freie Universität Berlin, Institute of Chemistry and Biochemistry – Biochemistry, 14195, Berlin, Germany*
[e] *Faculty of Health Sciences, Joint Faculty of the Brandenburg University of Technology Cottbus – Senftenberg, the Brandenburg Medical School Theodor Fontane and the University of Potsdam, Germany*

ARTICLE INFO

ABSTRACT

Here, we present a solid-supported membrane (SSM)-based electrophysiological approach to study sugar binding and Na^+/glucose cotransport by SGLT1 in membrane vesicles. SSM-based electrophysiology delivers a cumulative real-time current readout from numerous SGLT1 proteins simultaneously using a gold-coated sensor chip.

In contrast to conventional techniques, which mainly operate with voltage steps, currents are triggered by sugar or sodium addition. Sugar concentration jumps in the presence of sodium lead to transport currents between 5 and 10 nA. Remarkably, in the absence of sodium (i.e. no transport), we observed fast pre-steady-state (PSS) currents with time constants between 3 and 10 ms. These PSS currents mainly originate from sugar binding. Sodium binding does not induce PSS currents. Due to high time resolution, PSS currents were distinguished from transport and eventually correlated with conformational transitions within the sugar translocation pathway.

In addition, we analyzed the impact of driving forces on transport and binding currents, showing that membrane voltage and sodium concentration gradients lead to an increased transport rate without affecting sugar binding kinetics. We also compared Na^+/sugar efflux with physiologically relevant influx and found similar transport rates, but lower affinity in efflux mode.

SSM-based electrophysiology is a powerful technique, which overcomes bottlenecks for transport measurements observed in other techniques such as the requirement of labels or the lack of real-time data. Rapid solution exchange enables the observation of substrate-induced electrogenic events like conformational transitions, opening novel perspectives for in-depth functional studies of SGLT1 and other transporters.

1. Introduction

Diabetes is an expanding 21st century affliction of public health worldwide. Pharmacological targets aimed at treating this disease are of increasing interest among the scientific community. One target of major importance for the treatment of diabetes is the sodium glucose transporter SGLT1, which is responsible for the uptake of glucose from the intestine (Rieg and Vallon, 2018).

SGLT1 functions as a Na^+/glucose symporter. To pump glucose across the apical plasma membrane of epithelial cells, it requires a Na^+

gradient which is maintained by the Na^+/K^+-ATPase. A commonly used kinetic scheme for SGLT1-mediated transport is the 6-state alternating access model postulated by Parent et al. (Parent et al., 1992b) and further developed into an 8-state model by Loo et al., (2006). Both models assume that the accessibility of the substrate binding sites changes from inward facing to outward facing by a major conformational transition within the transporter, known as alternating access (Jardetzky, 1966). While the transition of the fully loaded carrier is supposedly evoked by sugar binding, membrane voltage is thought to control the transition of the empty carrier (Hazama et al., 1997; Loo

---

* Corresponding author.
E-mail address: andre.bazzone@nanion.de (A. Bazzone).
[1] The author contributed to the work equally and should be regarded as co-first author.

et al., 1998; Meinild et al., 2002; Parent et al., 1992a). One transport cycle begins with the outward facing empty carrier (C_{out}), which opens a cavity for sugar binding upon accepting two sodium ions ($C_{out}Na_2$) (Fig. 1A). Sugar binding ($C_{out}Na_2S$) then generates an occluded transporter intermediate ($C_{occ}Na_2S$), followed by the conformational transition to the inward facing, fully loaded carrier ($C_{in}Na_2S$). Both substrates are transported simultaneously. The sugar is released ($C_{in}Na_2$) followed by the two sodium ions. The empty carrier (C_{in}) may now relax to its outward facing conformation (C_{out}). Assuming saturating substrate concentrations and a negative membrane potential, the whole cycle completes in about 36 ms, resulting in a turnover rate of 28 sugar molecules per second (Loo et al., 2005).

Besides the major conformational transitions leading to alternating access, inner and outer gates control the accessibility of the sugar binding site within the inward facing and outward facing conformations (Wright et al., 2017). According to this model external sodium binds to the outward open conformation to open an external gate which then allows external glucose to bind, resulting in an ordered substrate binding. This model is supported by a vast amount of functional and structural data (reviewed in Ghezzi et al., 2018; Wright et al., 2011; Wright et al., 2017).

Translocation of sodium makes SGLT1 accessible for electrophysiological techniques. Those are neither in need of a synthetic fluorescent label, nor entail the downside of radioactive hazards. SGLT1 has been studied intensively using Two-Electrode voltage-clamp (TEVC) on oocytes (Eskandari et al., 2005; Hazama et al., 1997; Loo et al., 2005; Parent et al., 1992a). Most studies on SGLT1 rely on activation by

voltage steps in a voltage-clamp setting. The voltage dependence of SGLT1 originates from the apparent charge of the protein (Gorraitz et al., 2017; Loo et al., 2013): Voltage-induced steady-state currents have been attributed to the relocation of the negatively charged sodium binding sites via conformational transition within the empty carrier (C_{in} ↔ C_{out}) (Parent et al., 1992b). In addition, voltage-induced PSS currents have been measured which helped to distinguish multiple transporter intermediates within the sugar-free carrier (Loo et al., 2006).

Recently, we described a protocol for applying SSM-based electrophysiology to measure SGLT1 activity (Fig. 1B) (Bazzone and Barthmes, 2020). The superiority of SSM-based electrophysiology compared to other techniques for assaying transporter activity was recently discussed in a review (Dvorak et al., 2021). SSM-based electrophysiology is an innovative, well-established approach for cell-free electrophysiological characterization of electrogenic membrane transporters, e.g. transporters that catalyze net charge translocation across the membrane. In comparison to patch clamp, SSM-based electrophysiology achieves an enormous signal amplification enabled by a large sensor surface and the simultaneous measurement of transporters from several thousands of cells (Bazzone et al., 2017a). The high time resolution of a specially designed sensor type allows the detection of fast electrogenic PSS events. Instead of voltage steps, this technique relies on chemical substrate gradients to activate the transporter. Due to this key difference between SSM-based and conventional electrophysiology, we were able to observe SGLT1 PSS currents triggered by sugar binding for the first time (Fig. 1C). We observed electrogenic conformational transitions within the loaded carrier ($C_{out}Na_2S$ and $C_{out}S$), which – to our knowledge – have not been measured before.
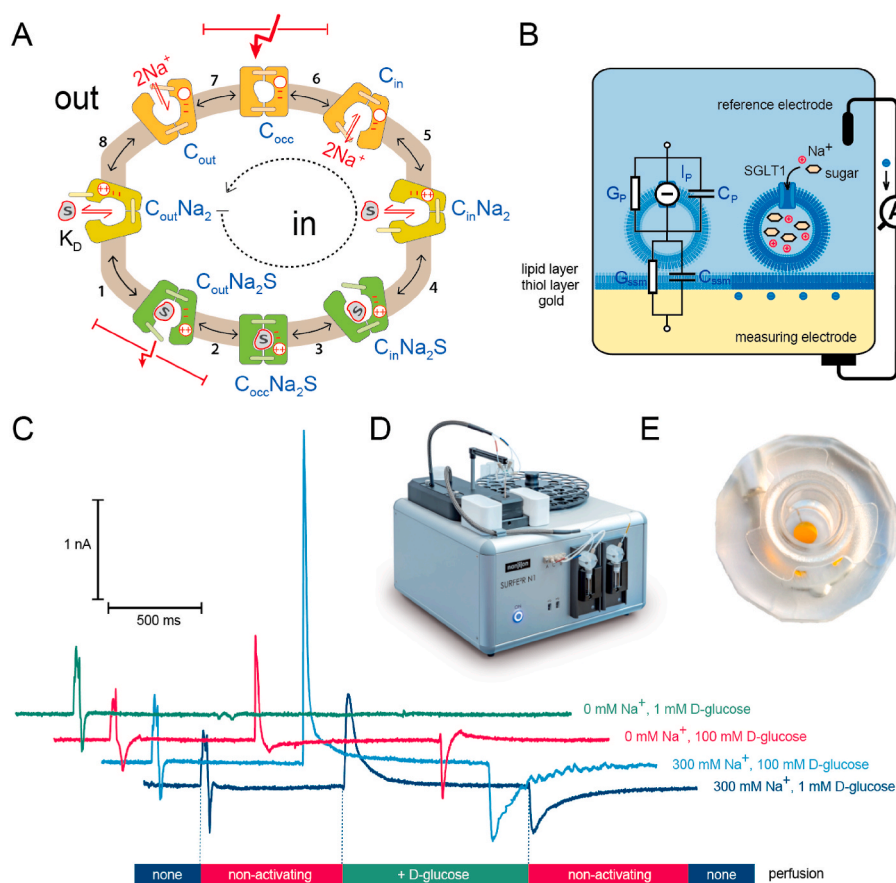

Fig. 1. SGLT1 investigated using SSM-based electrophysiology on the SURFE²R N1.
A) Transport model for Na⁺/sugar cotransport in SGLT1. The initial state of the carrier C is the outward facing, sodium-bound conformation ($C_{out}Na$). In SSM-based electrophysiology, the transport cycle is triggered by sugar binding upon sugar concentration jump (Reaction 1). Proposed electrogenic steps are indicated with red arrows. The major electrogenic step during transport is the alternating access of the empty carrier ($C_{in} → C_{occ} → C_{out}$) and sodium binding (Loo et al., 2013). Using SSM-based electrophysiology, a fast PSS current is detected upon sugar binding ($C_{out}Na_2 → C_{out}Na_2S → C_{occ}Na_2S$), even when no sodium is available (Figs. 1C and 2). **B)** Schematic representation of the sensor surface consisting of the SSM and the vesicular membrane sample containing SGLT1 forming a capacitively coupled membrane system on top of the gold electrode. **C)** Representative current traces using different sugar and sodium concentrations recorded from SGLT1 containing vesicles on SURFE²R N1 sensors with 1 mm diameter. A full trace is recorded during three perfusion phases: First, the sensor is rinsed with non-activating solution, generating a current baseline; second, a substrate concentration jump activates the transporter leading to a transient current which represents either a full or a partial transport cycle, depending on the experimental conditions; third the sensor is rinsed again with the non-activating solution to restore initial conditions. Usually, only the current recorded during the substrate concentration jump is analyzed. **D)** The SURFE²R N1 instrument consists of a measurement chamber holding the sensor and an open fluidic system allowing for the automated injection of up to 53 different measurement buffers. Measurements take place under continuous flow of solutions. **E)** SURFE²R N1 sensor with 3 mm diameter of the central circular active area. (For interpretation of the references to colour in this figure legend, the reader is referred to the Web version of this article.)

For our study we used purified membrane vesicles derived from CHO cells overexpressing SGLT1. Throughout assay development, we investigated the effect of different driving forces on the transport current and found that a sugar gradient is sufficient to measure SGLT1 using SSM-based electrophysiology. This allows for an easy and quick assay, which merely involves a single solution exchange to activate SGLT1. An additional sodium gradient or applied membrane potentials are not mandatory but further enhance the transport rate of SGLT1. In our standard assay the sugar concentration gradient is applied by a fast solution exchange, using symmetrical Na^+ concentrations inside and outside of the vesicles in absence of a membrane potential. For our assays, we have used the commercially available SURFE^{2}R N1 measurement platform (Fig. 1D and E).

We also identified and characterized PSS charge translocations, which must have a different origin than the previously measured voltage-induced PSS currents (Gagnon et al., 2007; Loo et al., 2005). Sugar binding, but not sodium binding triggers a PSS current in SGLT1. From the sugar induced PSS current, we deduct that sugar binds to SGLT1 at over-saturating concentrations even in the absence of sodium. Based on our results we conclude that SSM-based electrophysiology allows for new insights into SGLT1 electrophysiology and sugar binding in general.

2. Methods

A detailed description of the methods is provided in Supplementary Information (SI-M). It also contains the protocols for the radioligand transport assay and the orientation assay. SSM-based electrophysiology was performed using the SURFE^{2}R N1 as described in detail previously (Bazzone et al., 2017a; Bazzone and Barthmes, 2020).

2.1. Sample preparation

1 g of CHO cells overexpressing SGLT1 was harvested and disrupted by nitrogen decompression using a Parr cell disruption bomb at 70 bar. After removing cell debris by centrifugation (6,000 g, 4°C, 10 min), the plasma membrane was collected by ultracentrifugation (100,000 g, 4°C, 30 min). Plasma membrane vesicles were purified by ultracentrifugation (100,000 g, 4°C, 3 h) with a sucrose gradient (9 ml 45%, 9 ml 31%, 6 ml 9%). The upper band was collected and concentrated by centrifugation (100,000 g, 4°C, 30 min) to ~ 1–4 mg/ml total protein concentration. 10 μl aliquots were frozen in liquid nitrogen and stored at −80°C.

2.2. Sensor preparation

In brief, 1 mm or 3 mm sensors were thiolized with 1-octadecane-thiol (0.5 mM in 2-propanol, 30 min), before drying and coating by addition of 1.5 μl 1,2-diphytanoyl-sn-glycero-3-phosphocholine (DPhPC, 7.5 mg/ml in n-decane) and 50 μl of resting solution (composition varies for different assays according to Table 1).

2.3. Adding the sample to the sensors

One aliquot of membrane vesicles was diluted 1:10 in resting solution, and briefly sonicated using a tip sonicator (UP 50 H, Dr. Hielscher, equipped with MS 1 tip; 10 bursts, 20% amplitude, 0.5 s cycle time). Then 10 μl of the vesicles were added to the SSM by carefully submerging the pipette tip into the liquid. Sensors were centrifuged (2,000 g, room temperature, 30 min) before use.

2.4. Electrophysiological measurements

Technical details have been published recently (Bazzone et al., 2017a). In brief, the sensor wells with a capacity of 200 μl were inserted into the measurement chamber of the SURFE^{2}R N1. The integrated perfusion system automatically exchanged solutions above the sensor using a fast switching 3-way valve connected to a syringe pump. Two different solutions are injected to the sensor well from two different tubes that merge at a distance of about 10 cm above the sensor surface into one capillary of 0.8 mm in diameter. A continuous flow at a flow rate of 200 μl/s is enabled by adding solutions via that capillary at a distance of 0.5 mm from the sensor bottom and removing solutions from

Table 1
Summary of measurement solution compositions for all assays described in the main manuscript. The main buffer composition is given is 30 mM Tris/HCl (pH 7.5), 3 mM EDTA, 1 mM EGTA and 120 mM NMDG/SO4. Main buffer was split for each assay into two (NA + A) or three (NA + A + R) parts and components were added as given in the table.

No.	Assay	Reference figures	NA (external non-activating solution)	A (external activating solution)	R (internal solution)	Comments and variations
1	Influx	Figs. 1–5 (standard assay)	300 mM NaCl x mM Mannitol	300 mM NaCl x mM sugar	= NA	• In some experiments, sodium and potassium concentrations have been reduced to 60 mM (Fig. 3). • Sugar concentrations were 20 mM, 50 mM and 250 mM for different experiments. • For competitive inhibition, identical concentrations of a second substrate (MDG or D-glucose) were added to both, NA and A solutions (Fig. 2F).
2	Sugar Binding	Figs. 1–3	300 mM KCl x mM Mannitol	300 mM KCl x mM sugar	= NA	• KCl was replaced with CholineCl or RbCl in some experiments (Fig. 2C).
3	Efflux	Fig. 5	300 mM NaCl x mM sugar	300 mM NaCl x mM Mannitol	= NA	
4	Sugar Release	Fig. 5	300 mM KCl x mM sugar	300 mM KCl x mM Mannitol	= NA	
5	Influx (Na^+ gradient)	Fig. 4A–D	300 mM NaCl 250 mM Mannitol	300 mM NaCl 250 mM sugar	300 mM KCl 250 mM Mannitol	• During incubation in resting solution, the vesicles interior is kept sodium free.
6	Influx (membrane voltage)	Fig. 4E–K	300 mM NaCl 250 mM Mannitol	300 mM NaCl (x mM sugar + y mM Mannitol = 250 mM)	300 mM KCl 250 mM Mannitol	• During incubation in resting solution, the vesicles interior is kept sodium free. • The sensors were rinsed with 100 nM valinomycin, before performing this assay.
7	Influx (activation by Na^+)	Fig. 3	250 mM sugar 300 mM KCl	250 mM sugar 60 mM NaCl 240 mM KCl	= NA	
8	Na^+ binding (activation by Na^+)	Fig. 3	250 mM Mannitol 300 mM KCl	250 mM Mannitol 60 mM NaCl 240 mM KCl	= NA	

a second capillary at a distance of 5 mm from the sensor bottom. The order of solution flow is 1 s of non-activating (NA) solution, 1 s of activating (A) solution, 1 s of non-activating solution and 5 s of resting (R) solution. The currents were recorded in real-time using the SURFE^{2}R N1 Control Software v. 1.6.0.1. All experiments have been carried out at room temperature.

2.5. Solutions for electrophysiological measurements

Composition of NA, A and R solutions differ for each assay. Detailed buffer conditions for all assays are described in Table 1. In general, buffers consisted of 30 mM Tris/HCl (pH 7.5), 3 mM EDTA, 1 mM EGTA and 120 mM NMDG/SO$_4$. During the typical Na$^+$/sugar transport measurements, 300 mM NaCl was present in all solutions, and transport was initiated by exchanging 250 mM mannitol with 250 mM D-glucose. In sugar binding measurements, 300 mM NaCl was replaced with 300 mM KCl. A detailed explanation of buffer compositions for all assays is given in Table 1 and in Supplementary Information (SI-M).

2.6. Statistical analysis of electrophysiological data

Data presented here was recorded on SGLT1(+) and SGLT(−) vesicles purified from three different batches of cells across a time period of 18 months. This contributes to peak current variations across different datasets. All currents shown in one figure have been recorded from the same batch of vesicles. Standard deviations are obtained by averaging currents recorded from n different sensors with $4 \leq n \leq 10$. More details about reproducibility and signal stability are given in Supplementary

Information (SI-1, Figure SI-1). Recorded currents were exported as ASCII files for subsequent analysis using Microsoft Excel and Origin 2019.

3. Results

3.1. D-glucose triggers electrogenic binding and transport

To have a reliable and robust sample available on demand, SGLT1-expressing cells were used for preparation of membrane vesicles. These vesicles were utilized in all SURFE^{2}R experiments. As validation, radioactive uptake assays confirmed SGLT1 activity on a cellular level (Fig. 2A). As a strictly coupled Na$^+$/sugar symporter, SGLT1 requires both sodium and sugar to enable transport. When sodium was replaced by potassium the specific activity decreased to about 1% and was similar to the negative control (Fig. 2A). Using SSM-based electrophysiology, we performed 50 mM D-glucose concentration jumps in presence and absence of sodium (Fig. 2B). Each experiment consists of influx and efflux phases (Fig. 1C): At the end of each experiment, initial conditions are restored. However, only the current recorded upon the first solution exchange at t = 1 s is used for analysis. For a detailed explanation see Supplementary Information (SI-4).

We confirmed that sugar-induced currents are specific for SGLT1(+) vesicles and not observed in vesicles purified from a parental cell line not expressing SGLT1 (Fig. 2C, red). We use 3 mm sensors for higher signal-to-noise ratios (Fig. 2D), and 1 mm sensors for higher time resolution (Fig. 2E). The solution takes longer to spread across a 3 mm sensor than across a 1 mm sensor, and the decay time of the PSS current is
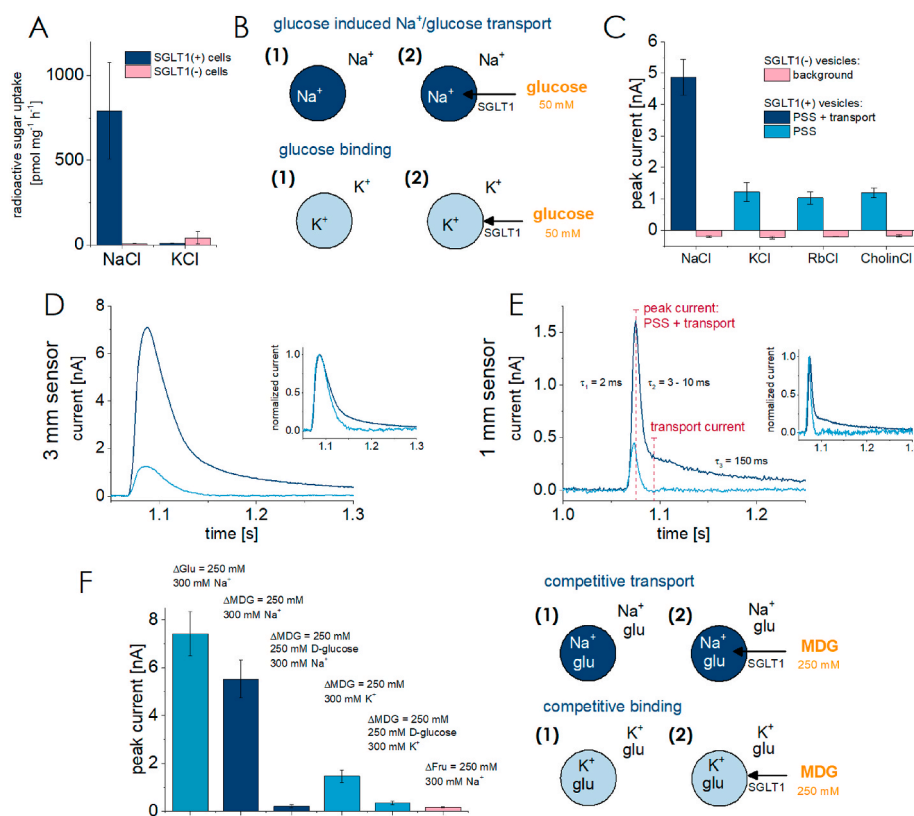

Fig. 2. Sugar-induced currents in the presence and absence of sodium.
A) Comparison of ^{14}C D-glucose uptake in radioactive uptake assay for SGLT1(+) cells (blue bars) and SGLT (−) control cells (red bars) when NaCl or KCl is used. No uptake is measured with KCl, indicating that the current measured in the absence of NaCl (figures A–D) is the result of a PSS reaction. **B)** Visualization of the experimental conditions used during the experiments shown in graphs C to D. The schemes show the different states of SGLT1(+) vesicles during each experiment in chronological sequence including the composition of the internal and external solutions. In the last state, SGLT1 is activated by a glucose concentration jump (labeled in orange) in the absence or presence of co-substrate. **C)** Comparison between peak current amplitudes upon 50 mM D-glucose concentration jumps obtained for SGLT1(+) vesicles (blue bars) and SGLT1(−) control vesicles (red bars) on 3 mm sensors when 300 mM of different chloride salts are used in all measurement buffers. **D)** transient currents triggered by 50 mM D-glucose concentration jumps in presence of 300 mM NaCl (dark blue trace) or 300 mM KCl (light blue trace) using 3 mm sensors. The inset shows both currents normalized to their peak current values. **E)** Same conditions as for B, but using 1 mm sensors allowing for higher time resolution. Average rise and decay times of the triphasic current in presence of sodium and time points to read-out PSS and transport amplitudes are indicated. **F)** Competitive inhibition of 250 mM αMDG-induced peak currents by 250 mM D-glucose in presence (dark blue bars) and absence (light blue bars) of 300 mM sodium. Both transport and PSS currents are inhibited. The red bar shows currents induced by 250 mM fructose in presence of 300 mM Na$^+$, which does not bind to SGLT1 and represents a negative control. The

green bar shows currents induced by 250 mM D-glucose in presence of 300 mM Na$^+$ as a positive control. On the right a visualization of the experimental conditions used during the competitive inhibition experiments is shown. Abbreviations: glu = D-glucose, MDG = α-methyl-D-glucose. (For interpretation of the references to colour in this figure legend, the reader is referred to the Web version of this article.)

limited by this solution exchange process (Bazzone et al., 2017a), requiring 1 mm sensors for more acurate kinetic measurements. Sugar-induced currents in the presence of sodium appear tri-phasic, when 1 mm sensors are used: (1) a fast current rise with $\tau_1 = 2$ ms (2) a fast current decay with $\tau_2 = 3$–10 ms and (3) a slow current decay with $\tau_3 = 150$ ms (Fig. 2E, dark blue).

In SSM-based electrophysiology all currents are transient. Substrate translocation charges the membrane on the sensor. The transport signal approaches zero when an electrochemical equilibrium is reached: membrane voltage acts as a counter force to the chemical substrate gradient leading to the current decay. Fast decaying currents typically represent PSS reactions within the transport cycle, whereas the current component with the highest decay time usually reflects transport and correlates to the steady-state current which is detected with other non-capacitive techniques (Seifert et al., 1993). We will therefore refer to the slow decaying current component as transport current.

When sodium is absent, no Na$^+$/sugar cotransport occurs. Hence, the transport current is not detected, leaving a mono-exponential instead of a bi-exponential current decay (Fig. 2E, light blue). The remaining PSS current components must represent a sugar binding induced reaction within the transport cycle which is observed in presence and in absence of sodium. We confirmed this hypothesis by further control experiments.

When using KCl, RbCl or CholineCl instead of NaCl, the PSS currents are not altered (Fig. 2C), thus these ions do not elicit any further electrogenic interactions with SGLT1. This is consistent with the observation that cation-coupled sugar transport is only observed with Na$^+$, Li$^+$ and H$^+$, but not with larger cations like K$^+$ (Panayotova-Heiermann et al., 1995).

Additionally, a competitive assay showed that α-MDG-induced currents recorded from SGLT1(+) vesicles – both in presence and absence of sodium – are inhibited when D-glucose was added beforehand (Fig. 2F). Also, fructose was proven not to be transported by SGLT1 (Tazawa et al.,

2005). Accordingly, fructose-induced currents recorded from SGLT1(+) vesicles are almost absent and similar to glucose-inhibited α-MDG-induced currents (Fig. 2F). These control experiments confirm that both PSS and transport currents originate from SGLT1.

The current signals resulting from SGLT1(+) vesicles in the absence of sodium, together with the control experiments described above, ultimately show that D-glucose interacts with SGLT1 in the absence of sodium, meaning D-glucose can bind to SGLT1 before Na$^+$ is bound. The higher current amplitude of the PSS current in the presence of sodium is due to a lower apparent sugar affinity in the absence of sodium (data not shown). But the binding process is fast, regardless of whether Na$^+$ was bound before the sugar or not, showing a rate constant of $1/\tau_2 \sim 200$ s^{-1}, which is within the range of the time resolution limit for the 1 mm sensors of the SURFE^{2}R N1. We conclude that sugar binding in SGLT1 is an electrogenic process allowing its detection using a label-free electrophysiological technique.

3.2. Sodium binding is not electrogenic

To investigate the molecular origin of the electrogenic PSS reaction, we performed sodium concentration jumps in the presence and absence of D-glucose to drive Na$^+$/sugar cotransport in SGLT1 (Fig. 3, red). There are three main differences in the experimental design compared to sugar concentration jumps: (1) the main driving force for transport now is the sodium gradient, (2) any PSS currents are triggered by sodium addition (sugar was made available beforehand), and (3) sodium jumps might trigger SGLT1-independent currents resulting from sodium-membrane interactions (Garcia-Celma et al., 2007) (false positive signals). We therefore subtracted the currents observed with SGLT1(−) vesicles (Fig. 3B/E) from those observed with SGLT1(+) vesicles (Fig. 3A/D) to calculate SGLT1-specific net currents (Fig. 3C/F).

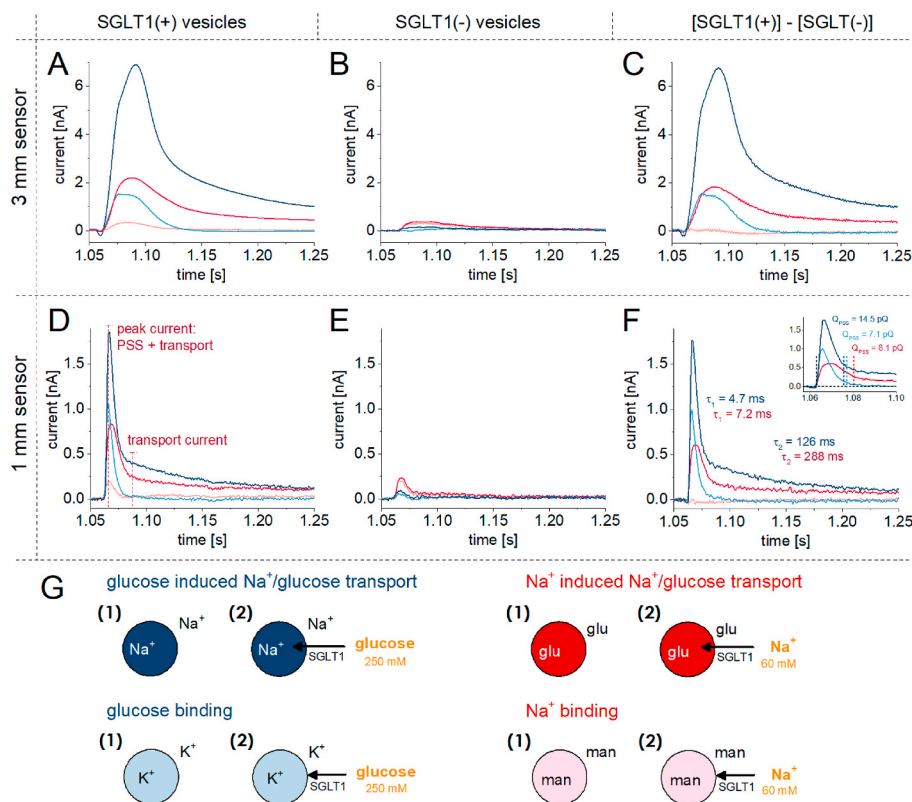We compared sugar concentration jumps in the presence and absence

Fig. 3. Comparison between D-glucose- and sodium-induced transient currents in presence and absence of co-substrate.
Results for 3 mm (A-C) and 1 mm (D-F) sensors are shown. Currents induced by 250 mM D-glucose concentration jumps (exchange for 250 mM mannitol, blue traces) in presence of 60 mM NaCl (dark blue traces) or 60 mM KCl (light blue traces) are compared to currents induced by 60 mM sodium concentration jumps (exchange for 60 mM potassium, red traces) in presence of 250 mM D-glucose (dark red traces) or 250 mM mannitol (light red traces). A/D) Transient currents induced on SGLT1(+) vesicles. For 1 mm sensors, the time points for read-out of PSS and transport amplitudes are indicated. B/E) Transient currents induced on SGLT1(−) control vesicles. C/F) Currents obtained by subtraction of SGLT1(−)-generated currents from SGLT(+)-generated currents. Time constants derived from biexponential fits of the current decays are indicated. The inset of Figure F shows the intervals for current integration to derive PSS charge translocation triggered by sugar or sodium binding when co-substrate was bound before. G) Visualization of the four different experimental conditions used during the experiments shown in graphs A and D. Abbreviations: man = mannitol, glu = D-glucose. The schemes show the different states of SGLT1(+) vesicles during each experiment in chronological sequence including the composition of the internal and external solutions. In the last state, SGLT1 is activated by glucose or sodium concentration jump (labeled in orange) in absence or presence of co-substrate. (For interpretation of the references to colour in this figure legend, the reader is referred to the Web version of this article.)

of sodium (Fig. 3, blue) with sodium concentration jumps in the presence and absence of sugar (Fig. 3, red). Final respective concentrations of sugar (0 mM or 250 mM) and sodium (0 mM or 60 mM) were kept the same across all experiments. The results clearly show that sodium does not generate any SGLT1-related PSS current in the absence of sugar (Fig. 3C/F, light red), while sugar does in the absence of sodium (Fig. 3C/F, light blue). Since sodium binding occurs in the absence of sugar (Chen et al., 1997), this renders sodium binding non-electrogenic. This also means we do not observe any sodium leak current through SGLT1 at 0 mV when the only driving force is the sodium concentration gradient (Fig. 3C/F, light red). Sodium leak currents have been observed previously upon voltage steps (Loo et al., 1999; Umbach et al., 1990) and lead to coupling coefficients of less than 2 under non-saturating conditions (Mackenzie et al., 1998).

While a biexponential decay was triggered by D-glucose addition in the presence of sodium (Fig. 3F, dark blue, $\tau_1 = 4.7$ ms, $\tau_2 = 126$ ms),

sodium-initiated currents are likewise biphasic and show similar time constants (Fig. 3F, dark red, $\tau_1 = 7.2$ ms, $\tau_2 = 288$ ms). However, PSS peaks upon sodium addition are significantly lower and only resolved by 1 mm sensors. Thus, sodium triggers part of the PSS reaction, when glucose has already bound to SGLT1. By integration of the PSS currents as indicated in the inset of Fig. 3F, we estimate that ~50% of the PSS charge translocation is triggered by sugar binding alone, while bound sodium allows to fully undergo the electrogenic conformational transition. This quantification only represents a rough estimation: Integration of sugar and sodium induced PSS currents in presence of co-substrate is error-prone, because transport currents overlap with PSS currents.

3.3. Impact of different driving forces on transport and binding

We investigated the impact of inward-directed sodium gradients and a negative membrane potential as additional driving forces when Na$^+$/
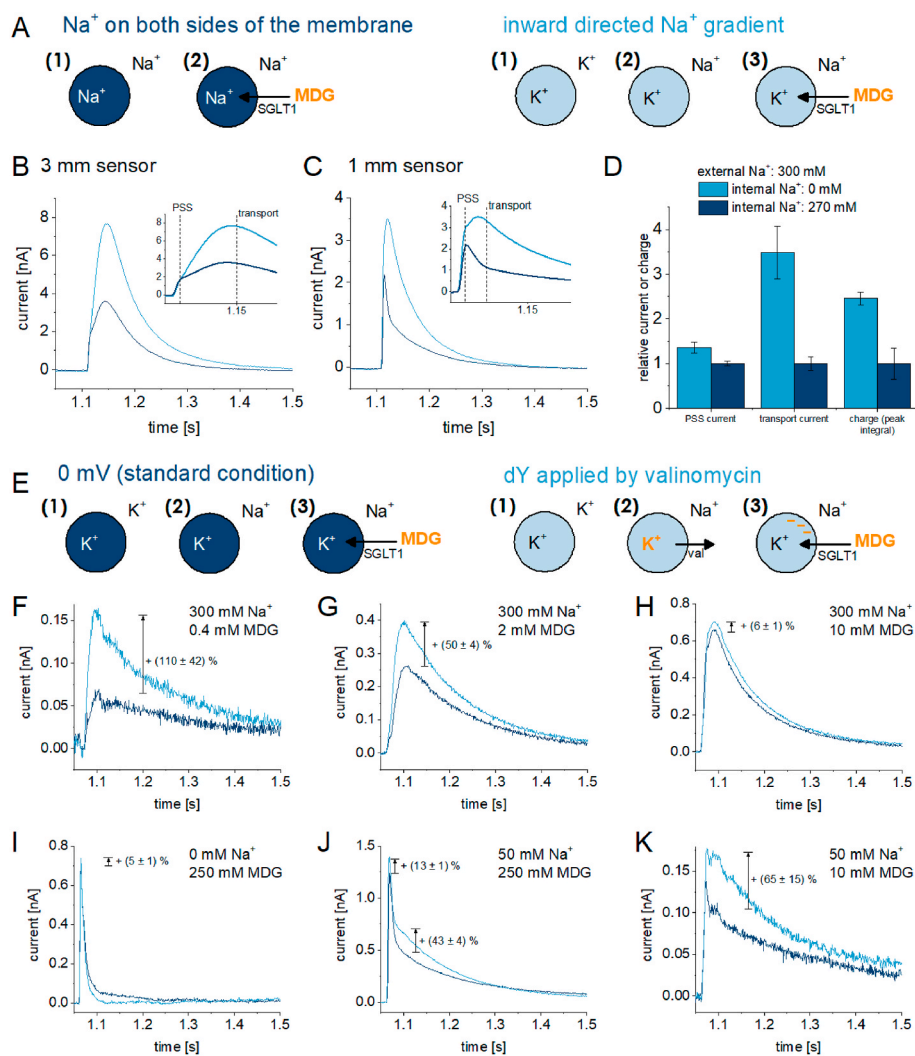

Fig. 4. **Impact of sodium gradients and voltage on Na$^+$/sugar cotransport and PSS currents**. The impact of sodium gradients is shown in A-D; The impact of voltage is shown in E-K. schemes (A,E) show the different states of the SGLT1(+) vesicles during each experiment in chronological sequence including the composition of the internal and external solutions. In the last state, SGLT1 is activated by a MDG concentration jump. **B-D)** Impact of an inward-directed sodium gradient on SGLT1 using 3 mm sensors (B) and 1 mm sensors (C,D), respectively. Comparison between transient currents recorded from samples containing SGLT1 when the vesicles have been loaded with 270 mM NaCl (30 mM KCl) (dark blue trace) or 0 mM NaCl (300 mM KCl) (light blue trace). External sodium concentration is 300 mM and identical for both conditions. Activation was performed by 250 mM αMDG concentration jumps in presence of the given sodium gradient, 300 mM → 270 mM and 300 mM → 0 mM respectively. The first concentration gradient is close to symmetrical conditions on both sites of the membrane. The internal sodium concentration is a result of diluting the Na$^+$-free SGLT(+) vesicles 1:10 in a buffer containing 300 mM Na$^+$ during sensor preparation. For each condition, the average currents from 6 sensors are displayed. Only the very first measurement from each sensor has been used for averaging to ensure that the ionic gradients in subsequent runs are not depleted after the sensor has been rinsed with Na$^+$ (see SI-3). The inset shows a zoom along the time axis and highlights the time points for read-out of transporter and PSS current amplitudes used for the bar plot (C). **D)** Bar plot showing the enhancement of transport currents, PSS currents and translocated charge (peak integrals) by application of an inward-directed sodium gradient (300 mM → 0 mM) compared to almost symmetrical conditions (300 mM → 270 mM). The results were obtained from 6 different 1 mm sensors. **F–K)** Impact of an inside negative membrane potential on SGLT1 at different sodium and sugar concentrations. The vesicles were loaded with 300 mM KCl (0 mM NaCl). All transient currents were recorded upon MDG concentration jumps in presence of x mM NaCl (300 – x mM Choline-Cl) in the external solution. Membrane potential was generated by addition of valinomycin leading to electrogenic efflux of potassium and an inside negative membrane po-

tential (see Figure SI-2). Transient currents were recorded using identical double solution exchange workflows before (no membrane voltage, dark blue trace) and after addition of valinomycin (membrane voltage, light blue trace). Graphs F–H show measurements at different sugar concentrations, and saturating sodium concentration. Graph I shows a measurement in the absence of sodium. Only PSS currents are recorded, which are not affected by the membrane voltage. Graphs J and K show measurements at different sugar concentrations with sodium concentrations in the range of the apparent K_M for sodium. (For interpretation of the references to colour in this figure legend, the reader is referred to the Web version of this article.)

glucose cotransport is triggered by a sugar concentration jump. Additional driving forces may increase the transport rate, either by accelerating the rate limiting reaction within the transport cycle (increasing V_{max}) or by increasing apparent affinity for sugar or sodium in the outward facing conformation (decreasing K_M).

3.3.1. V_{max} is increased in absence of internal Na^+

To further enhance the signal-to-noise ratio for the transport current, we performed a double solution exchange workflow with sodium-free SGLT1(+) vesicles (Na^+ was replaced by K^+), applying an inward-directed 300 mM Na^+ gradient 1 s before activating SGLT1 via a 250 mM MDG concentration jump (Fig. 4A). We compared the current traces under these conditions with our standard influx experiment, where SGLT1 was activated via a sugar concentration jump in the presence of ~300 mM Na^+ inside and outside the vesicles. Technical comments on the experimental design and the stability of sodium gradients are given in Supplementary Information (SI-3, Figure SI-4).

When using 3 mm sensors, in the presence of a sodium gradient, the peak current increases by a factor of 2 (Fig. 4B), and the transport component dominates the peak, leaving the PSS current invisible. Interestingly, in the absence of a sodium gradient, the PSS current was clearly visible within the biphasic current rise.

To better distinguish transport from PSS currents, 1 mm sensors were used (Fig. 4C). We found that the PSS peak current was not significantly affected by the sodium gradient, while the transport current and the overall charge translocation (peak integral) increased to $345 \pm 107\%$ and $322 \pm 135\%$, respectively, in presence of the sodium gradient (Fig. 4D). This supports our theory that the slow decaying current component reflects transport activity: High internal sodium concentrations will reduce the influx rate, since sodium release from the internal side of SGLT1 is known to be the rate limiting step in Na^+/sugar cotransport, when saturating substrate concentrations are used (Loo et al., 2006). The PSS component reflecting sugar binding to the outward facing conformation slightly decreases when sodium is available inside the vesicles. This may be attributed to a shift in the initial state of SGLT1: When sodium is available inside the vesicles, it may partially lock the transporter in the inward facing sodium bound conformation, reducing the population available for sugar binding at the external surface.

Comparison between the current signals in presence and absence of a sodium gradient also reveals that the peak currents obtained with 3 mm sensors are dominated by the transport current, while the peak currents obtained with 1 mm sensors are dominated by the fast PSS fraction of the signal. This is in agreement with the PSS currents decay times being limited by the time resolution of the solution exchange and the higher time resolution of the 1 mm sensors (Bazzone et al., 2017a).

3.3.2. Negative voltage increases apparent K_M for Na^+/sugar cotransport

We tested how a negative membrane potential affects transport and PSS currents. For the lack of direct voltage control, the potential is altered by chemical means. Vesicles loaded with 300 mM K^+ are incubated with 100 nM valinomycin. An exchange with K^+-free solution (containing 300 mM Na^+ instead) drives the electrogenic efflux of K^+ along its concentration gradient and generates a negative membrane potential. We validated the valinomycin-dependent K^+ efflux by comparing the current resulting from K^+/Na^+ exchange in the presence and absence of valinomycin (Figure SI-2).

A second solution exchange provides the sugar, which activates SGLT1-mediated transport in the presence of a membrane potential (Fig. 4E–K). For direct comparison, we carried out the same experiment on the same sensor before addition of valinomycin to measure SGLT1-mediated transport in the absence of a membrane potential. A negative membrane potential increases the transport current at non-saturating sodium and sugar concentrations (Fig. 4F,G,J,K), but not at saturating concentrations (Fig. 4H). This is in agreement with the previously described finding that V_{max} is not affected by voltage, while a negative potential increases apparent sugar and sodium affinity (Loo

et al., 2006; Parent et al., 1992b). Interestingly, the fast PSS current remains unaffected (Fig. 4I). A detailed discussion and further evaluation of voltage applications in SSM-based electrophysiology can be found in Supplementary Information (SI-2): As additional validation for this assay type, we analyzed the impact of membrane voltage on the H^+/sugar transporters XylE and LacY (Figure SI-3). For LacY only V_{max}, but not apparent K_M is increased upon application of voltage, which is in agreement with observations described in the literature (Kaczorowski et al., 1979).

3.4. Sugar efflux and release assays reveal asymmetric kinetic properties in SGLT1

To investigate if PSS currents are also triggered by sugar release or only by sugar binding, we performed negative glucose concentration jumps in the absence (release assay) or presence (efflux assay) of sodium to measure PSS glucose release or efflux, respectively.

3.4.1. Comparison of efflux and influx assays indicate transport symmetry

When sugar and sodium are present inside and outside the vesicles (efflux assay), the current observed upon external glucose removal shows no bi-exponential decay, but only the slow current component (Fig. 5B, red). In contrast to the influx assay both substrates are already bound to SGLT1 and efflux is triggered by sugar release upon solution exchange (i.e. sugar removal). The fast-decaying PSS current is either absent or smaller than during influx (Fig. 5B, blue).

When 250 mM glucose is used, the transport current observed in the efflux assay has an amplitude of opposite sign, but similar magnitude (-0.71 ± 0.17 nA) compared to the amplitude of the transport current in the influx assay ($+0.81 \pm 0.19$ nA). It can be concluded that V_{max} values in efflux and influx modes are similar. However, based on concentration-dependent transport currents we identify a slightly higher apparent affinity in the influx mode compared to efflux mode (Fig. 5C). K_M values were estimated to be below 10 mM in both cases. This is in agreement with K_M values for Na^+/glucose cotransport found in the literature, which range from 0.3 to 2 mM for influx (Díez-Sampedro et al., 2000; Hirayama et al., 1996; Hummel et al., 2011) and 7–60 mM for efflux (Eskandari et al., 2005; Quick et al., 2003; Sauer et al., 2000). Overall, the transport currents obtained in influx and efflux modes show similar characteristics, demonstrating the symmetry of kinetic transport properties in SGLT1.

3.4.2. Sugar binding rates are higher than sugar release rates

If sodium is absent, only PSS sugar binding and release are measured. As established, sugar binding triggers positive PSS currents (Fig. 5E, blue) with a decay time constant of $\tau = 9$ ms. In the release assay however, sugar is removed from its outward facing binding site, and we observe a fast-decaying PSS current ($\tau = 26$ ms) with negative sign (Fig. 5E, red). The apparent K_D values for sugar release and sugar binding in the absence of sodium (Fig. 5F) are similar and above 10 mM: The peak current increases by a factor of ~2.5 and 3.3, respectively, when D-glucose concentration is increased from 10 mM to 250 mM. Hence, the apparent affinity in the absence of sodium is lower than the apparent affinity for transport. This implies that cotransport is driven by optimized kinetics, rather than high sugar affinity. A similar conclusion is drawn from the currents recorded in the presence of sodium (Fig. 5B, blue): At lower sugar concentrations (10 mM instead of 250 mM), the peak current is reduced and shifts to the right. Hence, the PSS current fraction decreases while the transport component is unaffected when sugar concentration is reduced, indicating that the apparent K_D is higher compared to the apparent K_M, also in presence of sodium.

The integrals of the PSS currents reflect the translocated charge triggered by sugar binding and release. Sugar release ($Q = -18 \pm 3$ pC) appears slightly less electrogenic than sugar binding ($Q = 24 \pm 2$ pC), and at the same time about three times slower (rate constant k_{obs} of $1/\tau_2$ ~ 30 s^{-1} compared to $1/\tau_2$ ~ 100 s^{-1}). Taken together this explains the
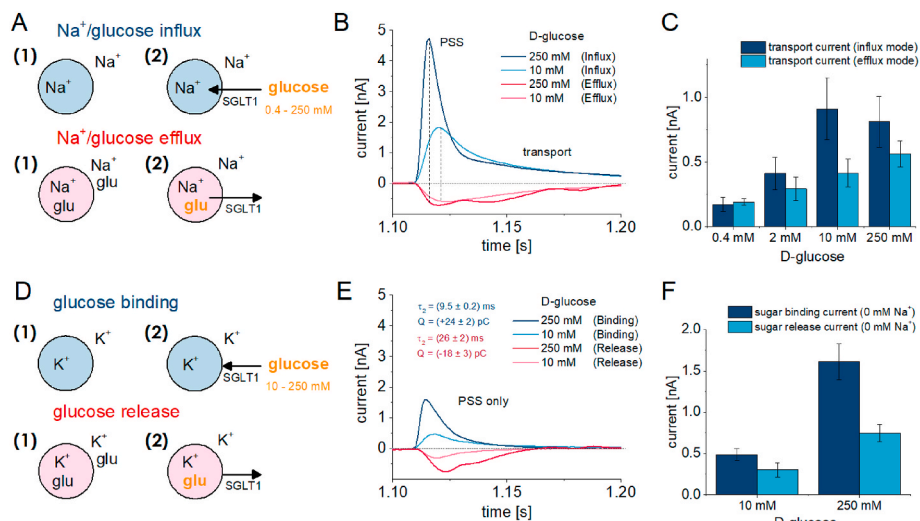
Fig. 5. Comparison between outward- and inward-directed Na$^+$/sugar cotransport currents and PSS sugar binding and sugar release currents. Transport currents are shown in A-C; PSS currents are shown in D-F. All current traces and bars reflect the average from six different sensors. **(A, B)** For the efflux transport assay (red traces), the SGLT1(+) vesicles were loaded with 300 mM NaCl and 250 mM or 10 mM D-glucose. The currents were recorded when switching to a solution completely free of D-glucose and thus inducing Na$^+$/D-glucose efflux out of the vesicles, driven by the outward-directed D-glucose gradient. For the influx transport assay (blue traces), SGLT1(+) vesicles were loaded with 300 mM NaCl. Influx currents driven by the inward-directed sugar gradient were recorded after 250 mM or 10 mM D-glucose concentration jumps in presence of 300 mM NaCl. **(C)** Average transport currents recorded from different sensors in influx and efflux modes for glucose concentrations ranging from 0.4 mM to 250 mM. The sign of the efflux currents is inverted for better visibility. **(D, E)** For the sugar release assay (red traces), vesicles loaded with 300 mM KCl instead of NaCl were subjected to the same negative glucose concentration jumps as in the efflux assay, but in absence of NaCl. Thus, only sugar release but not transport was enabled. For the sugar binding assay (blue traces), vesicles loaded with 300 mM KCl instead of NaCl were subjected to the same glucose concentration jumps as for the influx assay, but in absence of NaCl. Thus, only sugar binding was enabled. **(F)** Average PSS peak currents recorded from different sensors in binding and release modes (0 mM NaCl) for 10 mM and 250 mM glucose. The sign of the sugar release currents is inverted for better visibility. (For interpretation of the references to colour in this figure legend, the reader is referred to the Web version of this article.)

lower PSS amplitude observed upon sugar release compared to sugar binding. This results in the transport current dominating over the PSS current in efflux mode (Fig. 5B, red), as opposed to influx mode (Fig. 5B, blue).

4. Discussion

4.1. SSM-based electrophysiology opens a new perspective on SGLT1

We applied SSM-based electrophysiology to thoroughly study substrate binding and transport in SGLT1. The most frequently used method for this is the Two-Electrode voltage-clamp (TEVC) using oocytes (Loo et al., 2006; Parent et al., 1992a). Electrophysiology has the advantage of being a label-free technique. But TEVC is rather cumbersome and involves harvesting oocytes from frogs and injection of RNA. The size and shape of the oocytes makes it impossible to apply a fast solution exchange to activate transporters via substrate gradients. Patch-clamp is the gold-standard in electrophysiology, but not applicable for most transporters due to their low transport rates which result in poor signal-to-noise ratios. Here, we applied an emergent electrophysiological approach to achieve new insights into the biology of SGLT1.

The most important difference from conventional electrophysiology is how SGLT1-mediated currents are evoked. Classically, voltage steps are applied under various conditions to generate PSS and transport currents; initial conditions include a defined holding potential. Only voltage-induced PSS currents are measured. In SSM-based electrophysiology, SGLT1 is activated by sugar or Na$^+$ concentration jumps, and PSS currents must be a direct consequence of Na$^+$ and/or sugar binding.

Since experiments using SSM-based electrophysiology are performed at a floating potential and transport currents are usually detected at 0 mV, kinetic parameters can only be compared to results obtained with patch clamp or TEVC if the same voltage was used. It should also be noted that the driving forces define the measured properties of SGLT1, e. g. membrane potential, concentration of sodium and sugar at the inner and outer surface of the membrane as well as the sugar species. When kinetic parameters are compared across experiments, the driving forces need to be identical.

Here, we observed sugar-induced PSS currents in the absence of

sodium (Fig. 2C–E), although it is well accepted that sodium binds before sugar (Wright et al., 2017). However, to observe such currents, we needed to apply over-saturating sugar concentrations, about 20 times higher than the apparent K$_M$ for Na$^+$/D-glucose cotransport (Díez-Sampedro et al., 2000; Hirayama et al., 1996; Hummel et al., 2011). Therefore, our findings comply with the literature and the general assumption that sodium binds first under physiological conditions.

4.2. Sugar-induced PSS currents are not related to empty carrier translocation

Kinetic models have been applied to explain voltage step-induced transport and PSS currents observed with TEVC. Here, electrogenicity is assumed to occur only within the sugar-free carrier, e.g. conformational transitions within the empty carrier and external sodium binding (Loo et al. 2005, 2006). According to Loo et al. the empty carrier has an apparent valence of z1 = 0.7, while each sodium ion contributes an apparent charge of z2 = z3 = 0.15 (Loo et al., 2013). It is reasonable to question whether the origin of sugar-induced PSS currents is related to the same conformational transitions due to a sugar-induced shift in equilibrium between the intermediate states within the sugar-free carrier.

Interpretation of PSS currents involves assumptions about the predominant initial state of the transporter. Therefore, it is a requirement to know the orientation of the transporter within the vesicles, which has been determined using a site specific anti-SGLT1 antibody: We found that 97 ± 0.5% of SGLT1 molecules are in right-side-out orientation (Figure SI–2C). Hence, SGLT1 was activated from the extracellular side, in the outward-facing conformation (C$_{out}$), when performing substrate concentration jumps within the external medium in a typical SSM-based electrophysiology experiment.

Loo et al. assumed that in the presence of external sodium at 0 mV, the predominant state is outward facing, sodium bound (>78%) and the slowest step in the empty carrier translocation is 15 s^{-1} (Loo et al., 2006). The sugar-induced PSS currents we observed (k$_{obs}$ = 200 s^{-1}) would not be consistent with this if they resulted from empty carrier translocation (inward to outward), which needed to be rapid (~200 s^{-1}).

In contrast to sugar concentration jumps, sodium concentration

jumps do not trigger any PSS currents in the absence of sugar (Fig. 3), despite shifting the equilibrium from inward to outward facing conformation (Loo et al., 2006). This adds to the idea that empty carrier translocation itself does not cause PSS currents. In TEVC experiments, voltage steps seem to play the major role in these currents, rather than substrate interactions of SGLT1.

There are other key differences between voltage step and sugar-induced PSS currents, indicating that sugar-induced currents must have a different origin.

First, voltage applied in SSM-based electrophysiology does not affect amplitude or time constants of the PSS currents (Fig. 4I), whereas PSS currents observed with TEVC are triggered solely by voltage jumps and are therefore highly dependent on voltage (Loo et al. 2005, 2006).

Second, the PSS currents observed in voltage-clamp experiments are completely gone in the absence of sodium (Parent et al., 1992a). In SSM-based electrophysiology, in the absence of sodium a somewhat smaller sugar-induced charge translocation is measured (Fig. 2E), which has been mainly attributed to a lower sugar affinity in the absence of sodium. Absolute charge translocation is similar in the absence and presence of sodium at saturating sugar concentrations (data not shown). Hence, neither the positive charges of the sodium ions nor the negative charges of the empty sodium binding sites show a major contribution to the sugar-induced PSS charge transfer observed with SSM-based electrophysiology.

Third, sodium concentration affects the time constants of the PSS current measured in voltage clamp (Loo et al., 2005), but not in SSM-based electrophysiology (Fig. 2E).

Taken together, the origin of PSS currents in SGLT1 upon voltage step experiments observed in literature must be different from those observed upon sugar concentration jumps in SSM-based electrophysiology.

4.3. Sugar-induced PSS currents represent a conformational transition within the fully loaded carrier

We postulate that the sugar-induced PSS reaction is a direct consequence of sugar binding and release within the outward facing conformation. We observe either electrogenic closing or opening of the cavity triggered by positive or negative sugar concentration jumps. The electrogenicity may be a result of the movement of charged amino acids across the membranes axis. This can be viewed as an electrogenic 'induced fit' mechanism or electrogenic sugar occlusion and compared with the gating current observed for ion channels. The exact molecular origin of the sugar-induced electrogenicity remains unclear. Although a smaller PSS current has been detected when performing sodium concentration jumps in the presence of sugar (Fig. 3F, red), a major part of the PSS charge translocation is triggered by the sugar itself. Approximately 50% of the charge is only translocated if sodium is also available. Therefore, sodium needs to be present to fully undergo this electrogenic conformational transition - likely achieving a perfect 'induced fit' or occlusion of the sugar – or the charges of the bound sodium ions contribute to the electrogenicity of the same reaction.

Having investigated sugar binding and release (Fig. 5D–F), we suspect asymmetric kinetics for those two processes based on the observed rate constants k_{obs} ($1/\tau_2 \sim 30\,s^{-1}$ and $1/\tau_2 \sim 100\,s^{-1}$). Alternatively, the observation might be attributed to a shift in the initial state of SGLT1: In case SGLT1 accumulates in the inward facing conformation when glucose is available on both sites of the membrane, a lower number of SGLT1 molecules are able to directly release their sugar from the outward facing binding site upon sugar removal in the external solution. k_{obs} of sugar release would then be limited by the rates of preceding conformational transitions.

Recently, we also investigated bacterial H^+/sugar symporters and showed that under certain conditions – either with H^+ depletion or H^+ excess – transport is completely blocked, allowing us to study sugar binding, detected as a PSS current (Bazzone et al., 2016; Garcia-Celma et al., 2010). Surprisingly, these PSS currents show similar

characteristics to those detected with SGLT1: They are triggered by sugar binding and have rate constants in the range of 200–300 s^{-1}. In H^+/sugar transporters these PSS currents are also present when the H^+ binding sites have been neutralized by mutation. This undoubtedly shows for these H^+/sugar cotransporters that the electrogenicity of the PSS current must have a different origin than the transport current, which is assigned to the relocation of the negatively charged ion binding sites during alternating access of the empty carrier. Interestingly, the loosely coupled H^+/sugar transporter GlcP also shows similar sugar-induced PSS currents, even when sugar transport occurs in uniport mode (Bazzone et al., 2017b); And the bacterial Na^+/sugar cotransporter MelB shows PSS currents triggered by both, sugar and sodium binding (Ganea et al., 2011). The concept of electrogenic substrate binding might be applicable to sugar transporters in general and possibly to many other electrogenic transporters.

5. Conclusion

Conventional approaches to study SGLT1 such as TEVC apply voltage steps and produce electrogenic signals, which have been assigned to the empty carrier translocation and Na^+ binding/dissociation (Fig. 1A, steps 5–8) (Loo et al. 2005, 2006). Sugar-induced currents have not been measured, likely due to low time resolution when solutions are exchanged on the oocyte surface.

In contrast, SSM-based electrophysiology measures transporter activity triggered by substrate concentration jumps. Due to the high time resolution, we were able to identify a PSS reaction upon sugar binding which reflects a fast conformational transition following sugar binding and therefore contains kinetic information for the substrate bound carrier – the other half of the transport cycle, which has not been observed using TEVC (Fig. 1A, steps 1–4). *In vivo,* Na^+/sugar cotransport by SGLT1 is caused by a sugar concentration jump, i.e. food intake, whereas the membrane potential is kept constant. Hence, in SSM-based electrophysiology a native trigger for transporter activation is used. However, a clear limitation of SSM-based electrophysiology is the lack of direct voltage and temperature control, rendering TEVC and SSM-based electrophysiology complementary techniques.

Further studies are required to fully uncover the potential of this new read-out for sugar binding in SGLT1. Rate and equilibrium constants for the binding of different sugar substrates and inhibitors are now accessible in a label-free assay. In addition, charged residues may be neutralized by mutagenesis, which can alter the electrogenic PSS and help to understand the origin of this reaction.

CRediT authorship contribution statement

Andre Bazzone: Conceptualization, Methodology, Formal analysis, Investigation, Writing – original draft, Writing – review & editing, Supervision, Project administration. **Alexander Körner:** Methodology, Formal analysis, Investigation, Writing – review & editing. **Melanie Meincke:** Investigation, Writing – review & editing. **Manan Bhatt:** Investigation. **Srujan Dondapati:** Supervision, Project administration, Writing – review & editing. **Maria Barthmes:** Supervision, Project administration, Writing – review & editing. **Stefan Kubick:** Resources, Funding acquisition. **Niels Fertig:** Resources, Funding acquisition.

Declaration of competing interest

The authors declare the following financial interests/personal relationships which may be considered as potential competing interests: Authors AB, MB and NF are employed by Nanion Technologies GmbH, the manufacturer of the SURFE^{2}R N1 instrument used to compile the results described in this manuscript.

Acknowledgments

Appendix A. Supplementary data

Supplementary data to this article can be found online at https://doi.org/10.1016/j.bios.2021.113763.

References

Bazzone, A., Barthmes, M., 2020. Methods in molecular biology. Clifton, N.J.) 2168, 73–103.

Bazzone, A., Barthmes, M., Fendler, K., 2017a. Methods Enzymol. 594, 31–83.

Bazzone, A., Madej, M.G., Kaback, H.R., Fendler, K., 2016. PLoS One 11 (5), e0156392.

Bazzone, A., Zabadne, A.J., Salisowski, A., Madej, M.G., Fendler, K., 2017b. Biophys. J. 113 (12), 2736–2749.

Chen, X.Z., Coady, M.J., Jalal, F., Wallendorff, B., Lapointe, J.Y., 1997. Biophys. J. 73 (5), 2503–2510.

Díez-Sampedro, A., Lostao, M.P., Wright, E.M., Hirayama, B.A., 2000. J. Membr. Biol. 176 (2), 111–117.

Dvorak, V., Wiedmer, T., Ingles-Prieto, A., Altermatt, P., Batoulis, H., Bärenz, F., Bender, E., Digles, D., Dürrenberger, F., Heitman, L.H., IJzerman, A.P., Kell, D.B., Kickinger, S., Körzö, D., Leippe, P., Licher, T., Manolova, V., Rizzetto, R., Sassone, F., Scarabottolo, L., Schlessinger, A., Schneider, V., Sijben, H.J., Steck, A.-L., Sundström, H., Tremolada, S., Wilhelm, M., Wright Muelas, M., Zindel, D., Steppan, C.M., Superti-Furga, G., 2021. Front. Pharmacol. 12, 722889.

Eskandari, S., Wright, E.M., Loo, D.D.F., 2005. J. Membr. Biol. 204 (1), 23–32.

Gagnon, D.G., Frindel, C., Lapointe, J.-Y., 2007. Biophys. J. 92 (2), 461–472.

Ganea, C., Meyer-Lipp, K., Lemonnier, R., Krah, A., Leblanc, G., Fendler, K., 2011. Biochim. Biophys. Acta 1808 (10), 2508–2516.

Garcia-Celma, J.J., Hatahet, L., Kunz, W., Fendler, K., 2007. Langmuir : the ACS journal of surfaces and colloids 23 (20), 10074–10080.

Garcia-Celma, J.J., Ploch, J., Smirnova, I., Kaback, H.R., Fendler, K., 2010. Biochemistry 49 (29), 6115–6121.

Ghezzi, C., Loo, D.D.F., Wright, E.M., 2018. Diabetologia 61 (10), 2087–2097.

Gorraitz, E., Hirayama, B.A., Paz, A., Wright, E.M., Loo, D.D.F., 2017. Proc. Natl. Acad. Sci. U.S.A. 114 (46), E9980–E9988.

Hazama, A., Loo, D.D., Wright, E.M., 1997. J. Membr. Biol. 155 (2), 175–186.

Hirayama, B.A., Lostao, M.P., Panayotova-Heiermann, M., Loo, D.D., Turk, E., Wright, E. M., 1996. Am. J. Physiol. 270 (6 Pt 1), G919–G926.

Hummel, C.S., Lu, C., Loo, D.D.F., Hirayama, B.A., Voss, A.A., Wright, E.M., 2011. American journal of physiology. Cell physiology 300 (1), C14–21.

Jardetzky, O., 1966. Nature 211 (5052), 969–970.

Kaczorowski, G.J., Robertson, D.E., Kaback, H.R., 1979. Biochemistry 18 (17), 3697–3704.

Loo, D.D., Hirayama, B.A., Gallardo, E.M., Lam, J.T., Turk, E., Wright, E.M., 1998. Proc. Natl. Acad. Sci. U.S.A. 95 (13), 7789–7794.

Loo, D.D., Hirayama, B.A., Meinild, A.K., Chandy, G., Zeuthen, T., Wright, E.M., 1999. The Journal of physiology 518 (Pt 1), 195–202.

Loo, D.D.F., Hirayama, B.A., Cha, A., Bezanilla, F., Wright, E.M., 2005. J. Gen. Physiol. 125 (1), 13–36.

Loo, D.D.F., Hirayama, B.A., Karakossian, M.H., Meinild, A.-K., Wright, E.M., 2006. J. Gen. Physiol. 128 (6), 701–720.

Loo, D.D.F., Jiang, X., Gorraitz, E., Hirayama, B.A., Wright, E.M., 2013. Proc. Natl. Acad. Sci. U.S.A. 110 (47), E4557–E4566.

Mackenzie, B., Loo, D.D., Wright, E.M., 1998. J. Membr. Biol. 162 (2), 101–106.

Meinild, A.-K., Hirayama, B.A., Wright, E.M., Loo, D.D.F., 2002. Biochemistry 41 (4), 1250–1258.

Panayotova-Heiermann, M., Loo, D.D., Wright, E.M., 1995. J. Biol. Chem. 270 (45), 27099–27105.

Parent, L., Supplisson, S., Loo, D.D., Wright, E.M., 1992a. J. Membr. Biol. 125 (1), 49–62.

Parent, L., Supplisson, S., Loo, D.D., Wright, E.M., 1992b. J. Membr. Biol. 125 (1), 63–79.

Quick, M., Tomasevic, J., Wright, E.M., 2003. Biochemistry 42 (30), 9147–9152.

Rieg, T., Vallon, V., 2018. Diabetologia 61 (10), 2079–2086.

Sauer, G.A., Nagel, G., Koepsell, H., Bamberg, E., Hartung, K., 2000. FEBS (Fed. Eur. Biochem. Soc.) Lett. 469 (1), 98–100.

Seifert, K., Fendler, K., Bamberg, E., 1993. Biophys. J. 64 (2), 384–391.

Tazawa, S., Yamato, T., Fujikura, H., Hiratochi, M., Itoh, F., Tomae, M., Takemura, Y., Maruyama, H., Sugiyama, T., Wakamatsu, A., Isogai, T., Isaji, M., 2005. Life Sci. 76 (9), 1039–1050.

Umbach, J.A., Coady, M.J., Wright, E.M., 1990. Biophys. J. 57 (6), 1217–1224.

Wright, E.M., Ghezzi, C., Loo, D.D.F., 2017. Physiology 32 (6), 435–443.

Wright, E.M., Loo, D.D.F., Hirayama, B.A., 2011. Physiol. Rev. 91 (2), 733–794.